

Assessment of the PETase conformational changes induced by poly(ethylene terephthalate) binding

Clauber Henrique Souza da Costa¹ | Alberto M. dos Santos² |
 Cláudio Nahum Alves¹ | Sérgio Martí³ | Vicent Moliner³ | Kauê Santana⁴  |
 Jerônimo Lameira⁵ 

¹Institute of Natural Sciences, Federal University of Pará, Belém, Pará, Brazil

²Centro de Ciências Exatas e Tecnologias, Federal University of Maranhão, São Luis, Maranhão, Brazil

³Institute of Advanced Materials (INAM), Universitat Jaume I, Castellón, Spain

⁴Institute of Biodiversity, Federal University of Western Pará, Santarém, Pará, Brazil

⁵Institute of Biological Sciences, Federal University of Pará, Belém, Pará, Brazil

Correspondence

Jerônimo Lameira, Institute of Biological Sciences, Federal University of Pará, 66075-110, Belém, Pará, Brazil.

Email: lameira@ufpa.br

Kauê Santana, Institute of Biodiversity, Federal University of Western Pará, Santarém, Pará, Brazil.

Email: kaue.costa@ufopa.edu.br

Vicent Moliner, Institute of Advanced Materials (INAM), Universitat Jaume I, 12071 Castellón, Spain.

Email: moliner@uji.es

Funding information

Conselho Nacional de Desenvolvimento Científico e Tecnológico, Grant/Award Numbers: 306014/2018-1, 308254/2017-1, 402572/2018-1; Coordenação de Aperfeiçoamento de Pessoal de Nível Superior, Grant/Award Numbers: 88882.466102/2019-01, 88887.599350/2021-00; Generalitat Valenciana, Grant/Award Number: AICO/2019/195; Spanish Ministerio de Ciencia e Innovación, Grant/Award Number: PGC2018-094852-B-C21; Universitat Jaume I, Grant/Award Number: UJI-B2020-03

Abstract

Recently, a bacterium strain of *Ideonella sakaiensis* was identified with the uncommon ability to degrade the poly(ethylene terephthalate) (PET). The PETase from *I. sakaiensis* strain 201-F6 (*IsPETase*) catalyzes the hydrolysis of PET converting it to mono(2-hydroxyethyl) terephthalic acid (MHET), bis(2-hydroxyethyl)-TPA (BHET), and terephthalic acid (TPA). Despite the potential of this enzyme for mitigation or elimination of environmental contaminants, one of the limitations of the use of *IsPETase* for PET degradation is the fact that it acts only at moderate temperature due to its low thermal stability. Besides, molecular details of the main interactions of PET in the active site of *IsPETase* remain unclear. Herein, molecular docking and molecular dynamics (MD) simulations were applied to analyze structural changes of *IsPETase* induced by PET binding. Results from the essential dynamics revealed that the β 1- β 2 connecting loop is very flexible. This loop is located far from the active site of *IsPETase* and we suggest that it can be considered for mutagenesis to increase the thermal stability of *IsPETase*. The free energy landscape (FEL) demonstrates that the main change in the transition between the unbound to the bound state is associated with the β 7- α 5 connecting loop, where the catalytic residue Asp206 is located. Overall, the present study provides insights into the molecular binding mechanism of PET into the *IsPETase* structure and a computational strategy for mapping flexible regions of this enzyme, which can be useful for the engineering of more efficient enzymes for recycling plastic polymers using biological systems.

KEY WORDS

catalysis, environmental biotechnology, molecular dynamics, PETase, plastic, principal component analysis

1 | INTRODUCTION

Synthetic polymers, such as poly(ethylene terephthalate) (PET) revolutionized modern human civilization due to their versatile applications and low-cost production. However, due to the ultralong lifetimes of most PET-based plastic waste and the high resistance to biodegradation,^{1,2} these synthetic polymers remain one of the most challenging environmental problems with serious impacts on ecosystems and biodiversity.^{3–5}

Ideonella sakaiensis strain 201-F6 was recently discovered with the unusual ability to degrade and use synthetic polymers, such as PET, as its major energy and carbon source.⁶ This discovery opened up new scientific researches to find a solution for plastic waste using environmentally friendly alternatives based on enzymatic recycling in mesophilic temperatures.^{7–10}

Yoshida group demonstrated that *I. sakaiensis* express two closely related enzymes involved with PET degradation.^{6,11} The first enzyme is named PETase (PET hydrolase), which converts PET to mono (2-hydroxyethyl) terephthalic acid (MHET), bis(2-hydroxyethyl)-TPA (BHET), and terephthalic acid (TPA) as products. The second enzyme is the MHETase (MHET hydrolase) that further converts MHET into two monomers: ethylene glycol (EG) and TPA.¹² Structural and evolutionary studies of *I. sakaiensis* PETase (*IsPETase*) have shown that its structure resembles that of α/β -hydrolase enzymes.¹³ The α/β -hydrolase family includes lipases and cutinases, which catalyze the hydrolysis of fatty acids and cutin, respectively.^{13–15}

The PET-hydrolyzing enzymes were reported to be expressed in several organisms including fungi^{16–19} and bacteria^{20–22} that usually inhabit environments containing plastic debris or organic matters. However, although several structures of these enzymes have been reported recently, only a few of them are complexed with the PET polymer or its analogs.^{13,22–26} Thus, the PET-binding mode has been predicted mostly through computational methods.^{22,27}

The *IsPETase* binding site is larger when compared with thermostable cutinases, and also contains large hydrophobic residues, such as Trp156, important for substrate stabilization.^{13,28} Additionally, the PETase backbone does not show high conformational changes when bound to PET and the movements have been described as limited to the binding subsite.^{14,28}

Several studies have proposed a molecular mechanism for enzymatic catalysis.^{14,28,29} The conserved catalytic triad Ser160, Asp206, and His237 is present in the active site of the *IsPETase*^{13,14} and shares the same spatial orientation of α/β hydrolases enzymes. Figure 1 shows the *IsPETase* secondary and tertiary structures (PDB code: 6EQE), with its typical α/β -hydrolase fold containing two disulfide bonds (Cys203-Cys239 and Cys273-Cys289), which guarantee an extra rigidity to the protein structure, and 7 α -helices ($\alpha.1-\alpha.7$), 9 β -sheets ($\beta.1-\beta.9$), and 14 loops.

In the active site, a disulfide bond between the residues Cys176 and Cys212 is related to thermal stability.¹⁵ Moreover, the reduction of these cysteines results in a dramatic increase in the structural flexibility of the active site, thus destabilizing the integrity of the catalytic triad, which leads, consequently, to a decrease of the enzymatic

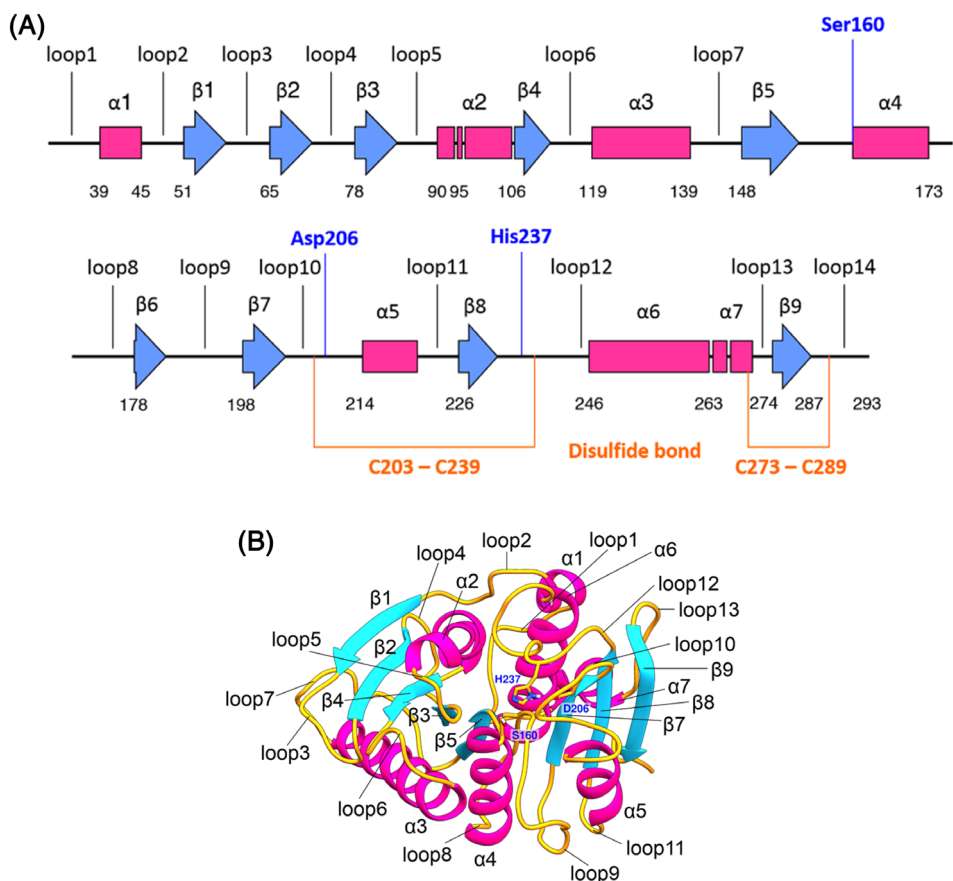


FIGURE 1 Schematic overview of the structure of *I. sakaiensis* PETase (*IsPETase*). **A**, The secondary structure of *IsPETase* with catalytic residues highlighted in blue and disulfides bonds of the cysteines in orange. **B**, Tertiary structure of *IsPETase* with the catalytic residues highlighted in blue.

activity.¹⁵ Despite its remarkable activity in the hydrolysis of PET polymers, the wild-type structure of the *IsPETase* is not optimized for full degradation of PET, and details of the catalytic mechanism of this reaction remain unknown.²⁴

One of the limitations of the use of PETase for PET degradation is the fact that it acts only at mild temperatures due to its low thermal stability. Indeed, the PET hydrolysis in *I. sakaiensis* was observed initially at 30°C.⁶ Nevertheless, *IsPETase* exhibits poor durability, where most of its activity is lost within 24 hours of incubation at 37°C.⁹ In addition, due to the inertness of PET at this temperature as a result of its intrinsic polymer properties, biocatalytic recycling at low reaction temperatures is unlikely to be feasible.³⁰ It is important to emphasize that protein flexibility is critical for enzymatic activity. Therefore, it is expected that the protein engineering should focus on mutagenesis residues far from the active site of this enzyme to increase the thermostabilization without causing impact in the flexible key regions of the protein that are critical for the hydrolysis of PET. Recently, Son et al have remarkably enhanced the thermal stability and improved the PET degradation ability of *IsPETase*.⁹ They have used the B-factor value as a parameter to map flexible regions of the protein far from the active site. Then, they explored some point mutations to increase the stability of the protein structure. The authors found that the β6-β7 connecting loop was a flexible region based on B-factor value and it was used as a target region of the protein for mutation.⁹ Indeed, point mutations have been used for stabilizing protein structure and some substitutions were proposed in flexible regions of the protein.³¹ Recently, Cui et al, have successfully redesign *IsPETase* to improve its robustness using a systematic clustering analysis combined with the greedy accumulation of beneficial mutations in a computationally derived library.³² Therefore, the thermal stability of PETase may be crucial for effective PET degradation and may provide biocatalysts as candidates for industrial PET recycling processes. In this work, we have examined in detail the protein conformational changes and residue fluctuations using essential dynamics to suggest potential target regions of *IsPETase* for mutagenesis. Currently, the binding mode of PET into the *IsPETase* subsites was not elucidated through experimental techniques due to difficulties in co-crystallization and low solubility of the entire polymer.^{13,14} In this sense, we have explored the binding mode of PET into the *IsPETase* subsites using computational approaches and we also compared with previous molecular docking analyses.^{13,15,24} Our computational results could shed light on further studies that aim to engineer its structure, to determine and improve its activity for the recycling of plastic polymers using biological systems.

2 | MATERIAL AND METHODS

2.1 | Molecular docking

Considering that the binding mode of PET in the *IsPETase* structure was not previously elucidated using experimental methods, we performed molecular docking of an oligomer consisting of four monomers

in their low free-energy conformations to analyze the selectivity and affinity of the polymer during the initial stages of the PETase catalytic process. Considering the wild-type structure of *I. sakaiensis* PETase (PDB: 6EQE, X-ray diffraction with 0.92 Å resolution) was the first reported mesophilic enzyme with affinity and catalytic activity against the PET,²⁴ we choose this structure with high resolution as a target to perform a detailed analysis of the interatomic interactions established between the protein and the PET.

To perform the molecular docking against the *IsPETase* binding subsites, we used the AutoDock Vina (version 1.1.2)³³ program with the following forms mimicking PET: monomer (bis-[hydroxyethyl] terephthalate, BHET), dimer (2-hydroxyethyl-(mono-hydroxyethyl terephthalate)₂, 2-HE(MHET)₂), and tetramer (2-hydroxyethyl-(mono-hydroxyethyl terephthalate)₄, 2-HE(MHET)₄).¹³ Conjecturing that the conformation of the PET tetramer in the *IsPETase* corresponds to that of individual monomers bound at *IsPETase* subsites I to IV, we sequentially constructed three models of PET: Model I comprises the individual PET monomers against four proposed binding subsites of PETase. In Model II, we combined two PET monomers, thus forming a dimer to dock against two adjacent *IsPETase* binding subsites. In Model III, we joined the four PET monomers forming a tetramer to dock against four potential adjacent PETase binding subsites (subsites I to IV). Table S1 shows the parameters used in the docking of the three models of PET.

The molecular docking in the AutoDock Vina was performed considering the flexibility of the residues from the subsites (Tyr87, Trp159, Ser160, Met161, Ile208, Asn233, His 237, Ser238, Asn241, and Arg280), as well as the flexibility of the ligand. The following Cartesian coordinates of the center of the docking grid, in Å, were applied: X = -0.51, Y = 4.23, and Z = 20.09; with dimensions of x = 70, y = 56, and z = 68 for PET flexible docking.

Further validation was performed using Molegro Virtual Docker (MVD)³⁴ and CSD-GOLD³⁵, then compared with the conformations obtained by the AutoDock Vina (available in Tables S1 and S3). After analysis and validation, the top-predicted pose of the *IsPETase*-PET complex obtained from AutoDock Vina was used as the starting point for the MD simulations.

2.2 | Molecular dynamics simulations

To evaluate the conformational dynamics of the *IsPETase*, we performed MD simulations in the Amber16 package³⁶ with structures derived from the docking study. The structure of *IsPETase* has two disulfide bonds (203-239 and 273-289) that play an important role in maintaining and stabilizing the protein structure. We performed MD simulations for two *IsPETase* systems: *IsPETase* in the unbound state (system I); and *IsPETase* in complex with PET tetramer (2-HE(MHET)₄) (system II). The simulation of polymers may be particularly difficult.^{37,38} Therefore, to obtain a satisfactory sampling of the PETase in the bound state, we applied restraint forces. This approach has been useful to identify domain motions especially for those of computational challenging systems.^{39,40}

First, the protein residues were parameterized with the ff99SB force field.⁴¹ The restrained electrostatic potential (RESP) protocol

was used to calculate the charges of PET tetramer using the Gaussian09 program⁴² with the Hartree-Fock method and the 6-31G* base set according to Amber protocol. The charges were then obtained using the antechamber module available in the Amber16 package. To describe PET structure complexed with *IsPETase*, the ligand was parameterized with the general Amber force field and the receptor (*IsPETase* enzyme) was parameterized with Amber ff99SB forcefield. Both systems were solvated in an octahedral periodic box of 12 Å side, with the TIP3P water solvation model.⁴³ The systems were neutralized with Cl⁻ ions to avoid unbalanced charges. The resulting systems were solvated with TIP3P water, where it was applied octahedral periodic boundary conditions. All stages simulations employed a nonbonded cutoff of 8 Å, where particle mesh Ewald (PME) approach computed the long-range Coulomb forces.

Prior to the MD simulation, the water molecules, ions, *IsPETase* structure were minimized with seven steps with 10 000 cycles of steepest descent and conjugate gradient algorithm to avoid clashes or improper geometries. We started the minimization with a constraint force equal to 500 kcal/mol/Å² applied in the cartesian coordinates, which was gradually decreased during minimization to relax the waters, counterions, protein, and ligand structure. Afterward, the systems were heated in 10 steps from 0 to 300 K. The first heating step was maintained at constant volume during 20 ps (0 to 100 K), from the second to the ninth step the temperature was gradually increased from 25 to 25 K until reaching 275 K with each step performed in a time of 1 ns for each step, and in the 10th step (last heating step) the system reached the temperature of 300 K. Then, we performed 5 ns of MD simulation to balance the density of the system and maintain a constant pressure (1 bar) and temperature (300 K). Here, we maintained the PET tetramer interacting with the *IsPETase* binding sites (I to IV) using a restraint force of 150 kcal/mol/Å² on the Cartesian coordinates of PET obtained from molecular docking. The SHAKE algorithm was applied for all hydrogen bonds in the analyzed systems. It is worth noting that restraint forces in the ligand structures in complex with the molecular receptor are widely applied to allow the conformational adaptation of the receptor structure to the ligands, thus, establishing favorable intermolecular interaction.^{44,45} It is important to highlight that the restraints force also increases the conformational stability of the complex throughout the MD simulation, avoiding the loss of the interaction between the investigated structures, and misinterpretation of the binding free energy values.^{46,47}

In the production stage of the unbound and bound systems (systems I and II, respectively), we performed 500 ns of MD simulations for each system using the NPT ensemble, and each system was replicated and assigned with different initial velocities to generate independent simulations.

2.3 | Principal component analysis and free energy landscape

The principal component analysis (PCA) is a technique that allows to reduce the dimensions of the analyzed trajectories during the MD

simulation of the covariance matrix (C), thus reducing the linear correlations between the spatial coordinates and converting them into a set of an orthogonal vector named principal component (PC) which describes the movements using the Cartesian coordinates X, Y, and Z of each analyzed atom.⁴⁸ This technique has been widely combined with MD simulations to evaluate the conformational changes of protein structures.^{40,49-55} Here, the CPPTRAJ module available in the Amber16 package was used to obtain the trajectories of *IsPETase* structures using the C_α coordinates over the 500 ns of MDs to generate the principal components (PC1, PC2, and PC3). The principal components that represent the protein movement are described according to Equation (1)⁵⁶⁻⁵⁸:

$$C_{ij} = \langle q_i q_j \rangle = \frac{1}{K} \sum_{k=1}^K q_i^k q_j^k \quad (1)$$

where, K is the configuration stored during an equilibrated MD simulation and q_i^k, as defined in Equation (2), is the internal mass-displacement of Cartesian coordinates x_i^k from i atom (i = 1,...,N; N = number of atoms from the molecule) with mass m_i, and the angular support represents the average obtained from the K configurations from the MD simulation after the equilibration.⁵⁶

$$q_i^k = \sqrt{m_i} (x_i^k - \langle x_i \rangle) \quad (2)$$

The diagonalization of the 3N × 3N covariance matrix C could be calculated (Equation (3)):

$$\Lambda = L^T C L \quad (3)$$

where, Λ is the diagonal matrix, which represents the relative contribution of each PC and contains the eigenvector, and L describes the matrix which contains the 3N orthonormal eigenvector Q_i. The eigenvalues show the mean square displacements (MSD) of C_α atoms, throughout the used eigenvectors, which describe the collective movement of protein⁵⁶⁻⁵⁸, and the diagonalization generates a reduced matrix with PC1, PC2, and PC3 for each frame obtained in MD simulation.

In the present study, we used the Bio3D package⁵⁹ to perform the PCA. Herein, the PCs were obtained from the diagonalization of the covariance matrix obtained from the Cartesian coordinates of the superposed C_α atoms of *IsPETase* structure. To avoid an underestimate of the atomic displacement, an iterated superposition procedure was applied before the PCA, where residues displaying the largest positional differences were excluded at each round until only the invariant “core” residues remained.⁵⁹

The analysis of the free energy landscape (FEL) was performed using the PC1 and PC2 using the terms of Equation (4):

$$\Delta G(PC_s) = -k_B T [\ln \rho(PC_1, PC_2) - \ln \rho_{\max}] \quad (4)$$

The Gibbs free energy involving the principal components PC1 and PC2 is referred to as $\Delta G(PC_s)$, which is in the function of the

probability distribution obtained from the MD trajectories, k_B is the Boltzmann constant, T is the temperature, ρ_{\max} is the probability of maximum value subtracted from the free energy value, contained in the most significant conformation, to approximate it to zero.^{60,61} To explore the conformations that are close to the native structure, the FEL values represented in two-dimensional were obtained from both probability distributions of PC1 and PC2 for all analyzed systems. To obtain the FEL plot and the conformational states of the PETase structure in the minimum of the energy landscape, we used the CPPTRAJ module of the Amber16 package. It is important to note that PCs were used to recognize the main structures that compose the first movement (PC1) and the second movement (PC2). We only considered the atomic coordinates of the bound and unbound states of the *IsPETase* structure to obtain the PCA plots to ensure the same amount of the analyzed atoms.

3 | RESULTS AND DISCUSSION

In the present study, molecular docking and MD simulations were employed to provide information on the structural conformations and movements of *IsPETase* induced by PET binding, as well as the selectivity and affinity of the substrate complexed with the *IsPETase* binding subsites.

Figure 2 shows the molecular docking obtained using the conformational search strategy of the monomers in the four *IsPETase* subsites based on previous studies,^{12,23} as described in the methods section. Our docking analysis demonstrated that the carbonyl oxygen of the PET ester group is positioned close to the nitrogen of the backbone amide group of the oxyanion hole (Figure 2). Figure 2A shows the binding mode of the four PET monomers analyzed separately, where the positioning of the monomer 1 (MHET moiety) formed π - π interactions with the aromatic amino acid Trp185 at the subsite (Figure S1), which were also observed previously observed by Han et al.¹⁴ The interaction distance between the Ser160 and the PET carbonyl is 5.88 Å. Panel B shows that the poses obtained for the dimers 1-2 and dimers 3-4 (Figure 2B) are similar to the individual monomers complexed at their respective subsites.

It is important to highlight that our analysis of MD simulations of the 500 ns of the *IsPETase*-PET complex revealed that the PET substrate formed a stable complex at the binding site and the distance between the Ser160-OG atom to the carbonyl group of the monomer 1 of PET showed an average distance of 5.88 Å over the MD simulation. These results are supported by previous studies²⁴ and it can be hypothesized that Ser160 could further approximate after its proton transfer to the His237, which is required for the nucleophilic attack on the carbonyl group.

The following interatomic distances of the *IsPETase* catalytic triad were found: between the oxygen (OG) from Ser160 and the nitrogen (NE2) from His237 was equal to 3.19 Å, and between the ND1 from His237 and OD2 from Asp206 was equal to 2.75 Å. Also, the results of the molecular docking showed intermolecular interactions via hydrogen bond of PET monomer 1 to the Ser213 (distance of 2.98 Å),

monomer 4 to the Ser236 (distance of 2.07 Å), and Thr279 (distance of 2.85 Å). Ala209 and Trp185 have interesting interactions with monomer1, Ala209 showed a π -alkyl interaction to the ring of monomer1, while Trp185 showed π - π interaction to the monomer1, showing an important role in the polymer positioning at the binding site during catalysis. The residues Ser214, Ile208, Pro210, Met161, His237, Asn241, Ser238, Cys239, Asn244, Gly235, Asn246, Ile232, Asn233, and Arg280 showed van der Waals interactions along with the PET polymer. Some molecular interactions are shown in Figure S1.

The structure obtained from the molecular docking also showed a similar binding mode to the PETase crystallographic structure in complex with MHET (PDB ID: 5XH3).¹⁴ Thus, indicating a satisfactory docking result for the subsite I. Detailed comparison between the pose obtained from the molecular docking and the BHET binding mode in the PETase crystallographic structure is shown in Figure S2.

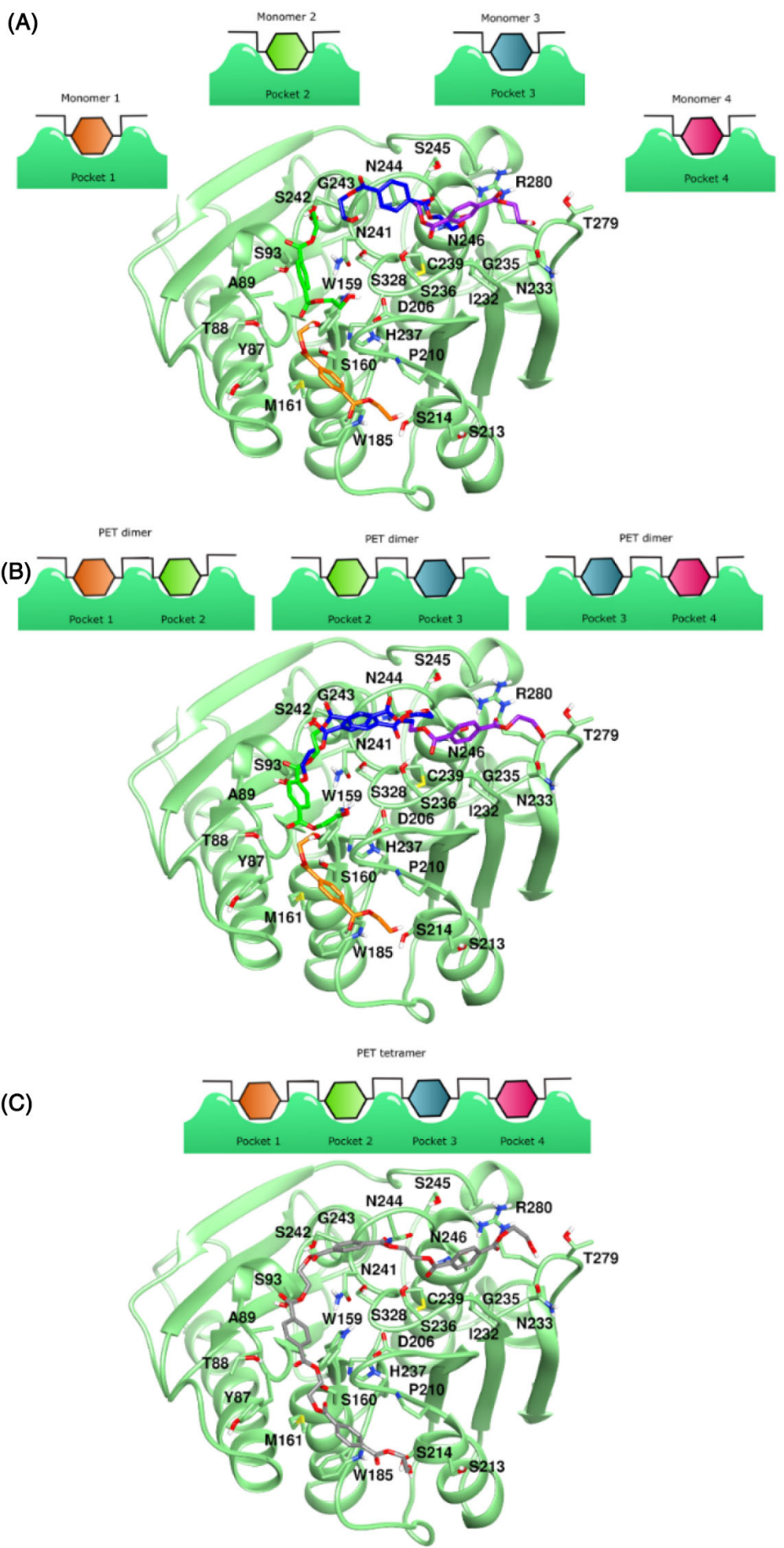
Figure 3 shows the electrostatic potential map of the crystallographic structure²⁴ used as a start point for the molecular docking simulation, where the highlighted region indicates the PET binding cavity (Figure 3A). The main residues for each subsite obtained by our docking results are shown in Figure 3B. The *IsPETase* subsites I-IV are proposed to accommodate four MHET moieties of the PET in an L-shape (Figure 3B,C). The complex was stabilized mainly by hydrophobic interactions. Hydrogen bond interactions with Ser236 and Asn246 were observed at the ester linkages between the MHET moieties. The residue Arg280 also participated in the interaction at subsite IV (Figure 3C), although it is demonstrated that its absence showed much greater PET degradation activity.¹⁴ Intermolecular distances between the atoms of the catalytic pocket and PET structure obtained from the molecular docking could be seen in Table S4.

The obtained binding modes (Figure 2C) demonstrated that the PET tends to fill the same spatial regions of the subsites as a monomer, dimer, or tetramer. Therefore, our *IsPETase*-PET complex represents a consistent and reliable model with favorable binding energies. The pocket mapping was compared with the docking results obtained from MVD³⁴ and GOLD³⁵ programs to validate our conformational search (see more in Table S2).

Previously, Fecker et al demonstrated that *IsPETase* has a binding mode similar to other PET-degrading cutinases, such as Cut2 obtained from *Thermobifida fusca* KW3 (TfCut2) and leaf-branch compost cutinase (LCC) obtained from a metagenomic survey.¹⁵ These authors explored the cutinases-PET complexes focusing only on the active site that contains the catalytic triad formed by the residues Asp179, His210, and Ser133.¹⁵ The comparison between *IsPETase* and cutinases TfCut2 and LCC demonstrated that the catalytic triad is conserved, showing the same spatial orientation in the three structures. Interestingly, the residues Asp179 and His210; and Ser133 and His210 formed hydrogen bond interactions in the active site. Our docking and MD simulations also demonstrated a very similar spatial orientation for these residues (Asp206, His237, and Ser160, respectively).

In contrast, Joo et al, investigated the interaction of four-MHET molecules mimicking the PET structure against four *IsPETase* binding pockets named subsite I, IIa, IIb, and IIc.¹³ According to their docking

FIGURE 2 Overview of the conformational search strategy applied in the docking simulations. A, Docking of individual monomers in proposed binding regions. B, Docking of dimers. C, Docking of the complete tetramer



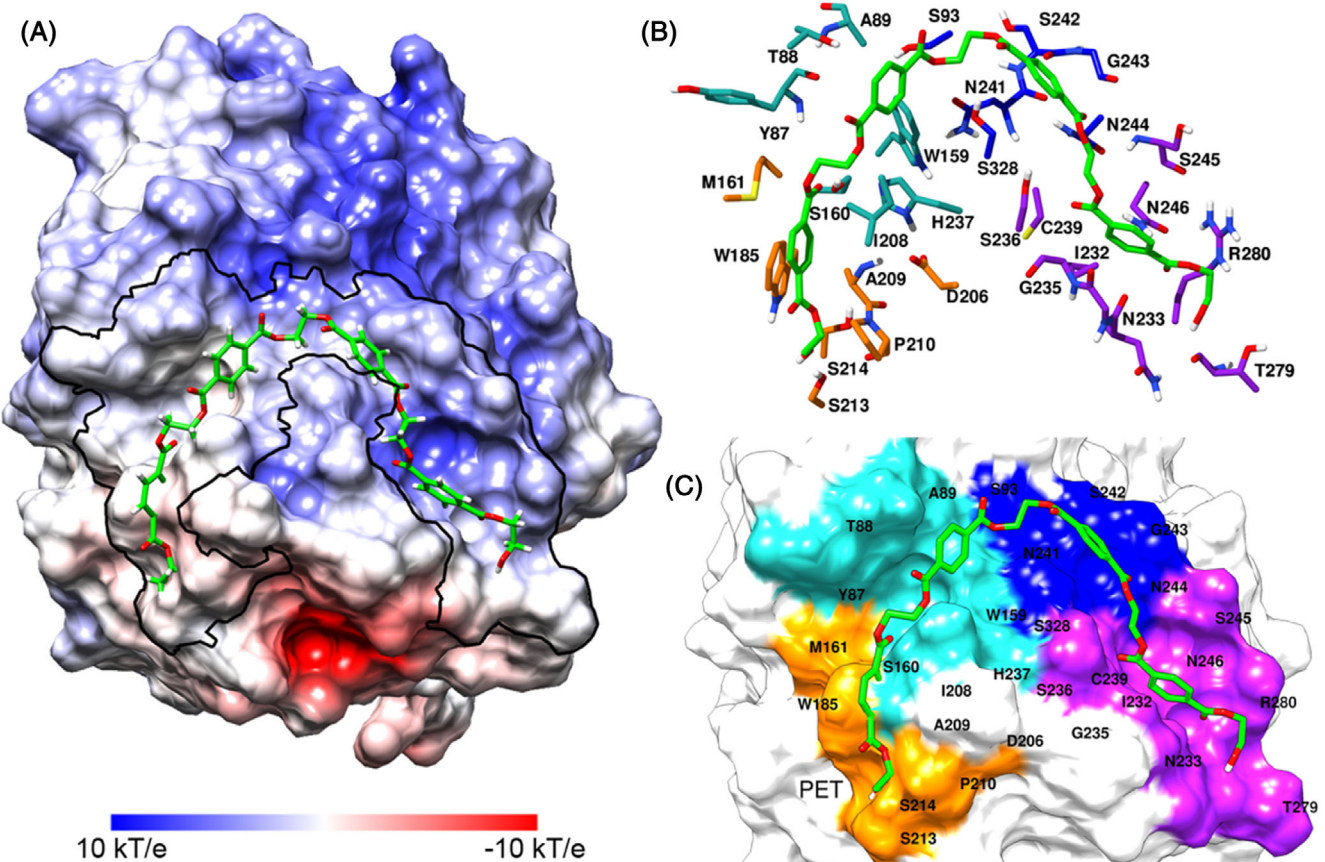


FIGURE 3 Binding mode of PET complexed with *lsPETase* and the molecular interactions obtained by the molecular docking simulations. A, Potential surface map for the crystallographic protein, where the highlighted region indicates the complete PET binding cavity. B, Residues belonging to the *lsPETase* binding subsites. C, Highlighted regions of each potential *lsPETase* binding site. Monomer 1 and subsite I in orange; monomer 2 and subsite II in green; monomer 3 and subsite III in blue; monomer 4 and subsite IV in purple

findings, the π - π interactions between Trp185 and the benzene ring of the first MHET moiety (~ 3.6 Å, subsite I) contribute greatly to the overall stabilization of the PET in the binding pocket. It was also demonstrated that Arg280 at the end of subsite IIc, due to its protruding shape, hinders stable interaction of *lsPETase* with PET substrate beyond the fourth moiety, and its substitution into a small hydrophobic residue might allow more stable binding for a longer substrate. Similarly, Austin et al used docking simulations to predict the PET binding mode in the *lsPETase* and demonstrated that PET formed an interaction with the nucleophilic hydroxyl group of Ser160 (~ 5.1 Å) and the His237 is positioned within 3.9 Å of the Ser160 hydroxyl.²⁴ The interatomic distances obtained from our simulations are consistent with this previous proposal and also with the previous results reported by Fecker et al and Joo et al.

3.1 | Analysis of molecular dynamics of *lsPETase*

Our model of the *lsPETase*-PET complex started with a consistent binding mode as previously proposed in docking studies.^{13,24} In the present study, we used MD simulations to explore the conformational change of *lsPETase* upon PET binding. The RMSD plots of the

lsPETase structure in the unbound and bound states are shown in Figure S3. Our MD simulations protocol successfully sampled the difficult-to-access configurations of the *lsPETase* structure in complex with PET, showing high stability during the MD simulation, with deviations below 3.0 Å (Figure S3A). In general, the *lsPETase* in both bound and unbound states showed no significant atomic RMSD deviation over the MD trajectory, exhibiting RMSD values of 1.93 ± 0.43 Å and 1.56 ± 0.35 Å, respectively (Figure S3B and Table S5). Thus, further analysis to better describes the differences between the unbound and bound systems was carried out using more detailed analysis.

The analysis of the binding mode of PET complexed with PETase showed that the Trp159 from the subsite II formed a π - π stacking interaction with the aromatic ring from the MHET moiety (see Figure S1). Furthermore, the Ile209 formed a π -alkyl interaction with the same structural moiety of PET located at the subsite II. Regarding subsite I, we noted that residue Trp186 (NE1) formed H-bond interactions with the oxygen atoms of the MHET moiety (O11, O13, and O14). We conjecture that these interactions are responsible to maintain the PET in subsite I and II over the MD trajectory. Differently, the subsites III and IV, the structural moieties of PET formed numerous hydrophobic contacts that weakly maintain the PET structure in the pocket. Thus, its structure suffers considerable conformational

changes that lead to its departure from the cavity. Figure S4 shows an overview of each MHET moieties (hexagons) complexed at their respective binding subsite during MD simulations.

Monomer 2 showed the most stable interactions in the elected binding subsites (system II, Figure S4). In contrast, the monomers located at the ends of the PET polymer (monomers 1 and 4) showed higher mobility. The RMSD plot also showed that the use of a restraint force to maintain the PET in the binding subsite allowed protein adjustments for a better fit during the first frames of the MD trajectory. When the restraint force was reduced, the PET conformation was gradually adjusted and remained in the subsite until the end of the 500 ns of simulation.

We also analyzed the root-mean-square fluctuation (RMSF) for individual amino acid residue over the 500 ns of MD simulation. This analysis was used as a criterion for quantifying the flexibility of *IsPETase*, where higher RMSF values correspond to more flexible regions of the protein during MD simulation. The RMSF shows that the catalytic residues Asp206 and His237 located at β 7- α 5 and β 8- α 6 connecting loop, respectively, presented considerable mobility during MD simulations. It is interesting to note that previously, Fecker et al analyzed the conformational changes of *IsPETase* over time, as well as the interactions of PET at the subsites; and they found that the β 7- α 5 loop (loop10) flexibility was larger in *IsPETase* than in its close cutinase homologs.¹⁵

3.2 | Essential dynamics of *IsPETase*

The use of *IsPETase* for PET degradation is limited due to its low thermal stability. Thus, we have used essential dynamics to identify the flexible regions in the protein structure. These flexible regions in the *IsPETase* can be used as a potential target for enhancing thermal stability. Besides, this analysis can also provide insight into the induced-substrate conformational change in *IsPETase*. Herein, we performed a PCA for the two analyzed systems: (a) PETase in the unbound state (ligand-free), and (b) *IsPETase* in the bound state.

Corroborating with PCA results, the residue Trp185 showed a considerable fluctuation between unbound and bound states (Figure 4). Curiously, the characteristic of the conformational movements of the Trp185 is directly related to the accessibility of the PET polymer since its fluctuation modifies the cavity and adjusts the

monomer 1 accommodation at the binding site. Also, the movement of Trp185 possibly controls the subsite entrance of a new PET monomer in the binding subsite, thus leading to continuous depolymerization.²⁴ Moreover, during the MD simulation, the Trp185 showed different conformations that increase the cavity volume of the monomer 1 to accommodate the polymer (Figures S5 and S6), as previously observed.²⁴

These variations indicate that the protein alters its conformation to receive the substrate. It also indicates that Trp185 is involved in the permanence of the PET monomer in the first binding subsite of the enzyme as previously proposed.¹⁴ In the bound state (Figure S7), the Trp185 residue position, as well as all the catalytic residues of the protein, remained stable. This behavior could be associated with the catalytic residues exerting significant interactions with the ligand.

However, the permanence of PET in the binding subsite may impose local structure fluctuation, particularly, on the residue Trp185. This behavior was also observed for Ser160, the main catalytic residue. Moreover, the interaction of PET tetramer in the binding subsite causes a displacement of the residue Asp206 located at the β 7- α 5 connecting loop. Conformational changes can play a crucial role in regulating the PET binding to the hydrophobic subsites and in the control of the catalysis. We noticed in the PCA analysis that the residues Asp206 and Trp185 are very flexible. The results also show considerable fluctuations in the residue His237 at β 8- α 6 connecting loop. Then, we conjecture that these residues are key residues for the mechanism of binding and release of PET.

PCA result also shows that the most flexible region of the protein is located at β 1- β 2 connecting loops for both systems *IsPETase* in the unbound and the bound states (Figure 4). It is worth noting that these essential dynamics involve almost 37.8% and 25.6% of the motion of the unbound and in the bound systems, respectively (see Appendix S1). The results also reveal that participation in the conformational flexibility of β 7- α 5 and β 1- β 2 connecting loop is higher in *IsPET-PETase* complex than in *IsPETase* without ligand. Therefore, we suggest that the β 1- β 2 connecting loop may be targeted for mutagenesis to increase the *IsPETase* stability since it is located far from the active site.

Initially, we started the MD simulation assuming the PET L-shape as the most probable conformation for the *IsPETase*-PET complex, as previously suggested in other studies.^{13,24} However, Wei et al indicated that the amorphous PET is highly stiff and its binding into the

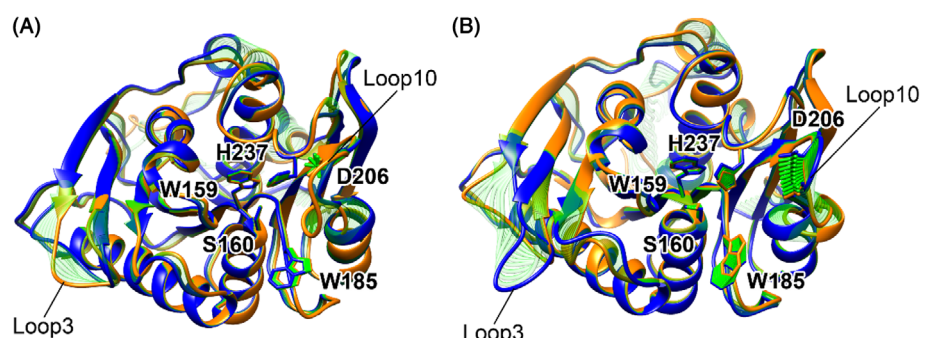


FIGURE 4 Essential motion described by the first principal component (PC1) of each analyzed *IsPETase* structure: (A) *IsPETase* in the unbound state, (B) *IsPETase* in the bound state. Loop3 and Loop10 corresponding to β 1- β 2 and β 7- α 5 connecting loops, respectively. The essential dynamics were obtained from 500 ns of MD simulations

four *IsPETase* subsites is unlikely.⁶² To assess the existence of different conformations acquired by PET over the MD simulation, we performed a clustering analysis in the Cpptraj⁶³ program using as data set the spatial coordinates calculated through the RMSD values to investigate the collective variable for the PET conformations sampled over the 500 ns MD simulations. We obtained a hierarchical agglomerative clustering with five clusters using as linkage the average-linkage.⁶⁴ The average values of the pseudoreplicates using F-statistic (pSF)^{64,65} and Davies-Bouldin indexes (DBI)^{64,66–68} were equal to 9072.386670 and 0.9566, respectively. The comparison between the planar (green) and L-shape (cyan) conformations of PET structure analyzed over 500 ns of MD simulations is depicted in Figure S7. Our clustering analyses showed that the L-shape corresponds to approximately 1% of the conformations acquired by PET and the planar shape corresponds to the most common conformation with a frequency of approximately 97.2% (see Table S7), which is most correlated with the findings reported by Wei et al.

3.3 | Free energy landscape analysis of *IsPETase*

As commented in the Introduction section, experimental works have suggested the PETase backbone does not present high conformational changes upon PET binding, since its movement is limited to the binding subsite.^{14,28} Indeed, our PCA results show that the main movement of *IsPETase* is associated with β 7- α 5 and β 1- β 2 connecting loops motion. Since PCA describes the largest amplitude protein motions during a simulation, the bi-dimensional free energy landscape (FEL) was obtained taking into consideration the bidimensional projections of PC1 versus PC2, which are considered the coordinates used for obtaining the FEL. The FEL of *IsPETase* in the unbound state showed that at the beginning of the MD, the conformations acquired by the *IsPETase* structure were similar to those obtained at the end of the simulation, thus demonstrating that conformational states of the *IsPETase* were not altered dramatically over the MD trajectory, which is in agreement with previous experimental data.^{14,28} We also observed for the analysis of the PCA_{PC2vsPC3} and PCA_{PC1vsPC3} plots, a conformational dispersion at the end of MD simulation that not formed isolated clusters. It is important to note that the conformations of the PC1 were not directly correlated with those found in PC3, thus demonstrating that the initial conformations were grouped separately from the other conformations that do not contain the PET at the binding site (see Figure S9).

The main difference between the most stable structure of *IsPETase*-PET complex (P1 in Figure 5) and *IsPETase* in the unbound state (P4 in Figure 5) is in the β 7- α 5 connecting loop, where we noted that the Asp206 opened the cavity of the active site. Other conformational states with high probability were described for the unbound state with P2 with a reduced cavity and P3 with an opened cavity similar to that of P1 (Figure 5A). Considering that the structural engineering of *IsPETase* using site-direct mutagenesis has led to optimized catalysis of PET,^{13,25,69} finding the most stable conformation of its structure is an important task for the

improvement of its active site selectivity and also to better understand the conformational mechanism of the enzyme that influences in the catalysis.

The *IsPETase* has large regions with polar surface charges with few regions with acidic residues (red surfaces, Figure S10). In the subsite of monomer 1, more neutral regions are observed, while for the other monomers regions high hydrophobic surfaces are detected. There is an increase of the cavity's volumes (see Figure S6) of the subsites when the *IsPETase* structure is complexed with the PET, demonstrating conformational conservation of the catalytic triad. It is important to point out that the wide cleft in the active site would be necessary to accommodate semi-aromatic crystalline polyesters.²⁴ Recently, Knott et al studied the catalytic mechanism of the MHETase enzyme converting MHET to terephthalic acid and ethylene glycol.⁷⁰ The authors demonstrated that the main domain of MHETase is similar in the residue composition to *IsPETase*, which suggests insights into the hydrolysis mechanism of PET performed by the *IsPETase*.⁷⁰ However, the mobility of key residues and loops during the binding and catalysis remains unclear. Our analyzes of FEL revealed an increase in *IsPETase* stiffness upon binding of PET, which suggests that binding of PET gives rise to an effective motion of β 7- α 5 connecting loop, which could have a direct influence on the PET binding and catalysis. In particular, we suggest that the rearrangement of this loop may be relevant for enabling the adoption of a proper conformation for PET recognition.

The comparison of *IsPETase* states analyzed in the FEL plots (see Figure 5 and Figure S11), revealed that the P1 (unbound) and P4 (bound) states demonstrate that the main conformational change in the transition between the unbound state to the bound state is associated with β 7- α 5 connecting loop, which that exhibits movements of the residue Asp206 (see Figure S11). In P1 (Figure 5, PETase free), this residue interacts with His237 through hydrogen bond (1.78 Å) in *IsPETase* in the unbound state. While the mobility of the β 6- β 7 connecting loop is associated mainly with the residue Trp185, which has a fluctuation in the change of states, while important catalytic residues, such as Trp159, Ser160, and His237 remain in stable conformations (see Figure 5C,D, and Figure S11).

Considering that the conformations located at the minima have similarities to each other, we found that the conformations in P2 and P3 of the *IsPETase* in the unbound state demonstrated a similar conformational change in the connecting β 7- α 5 loop (loop 10) to accommodate the PET substrate (Figure S11A). The minimum conformations of *IsPETase* located at the P5 and P6 showed the PET structure in two conformations, that is, a planar and L-shape configuration, respectively. The positions of His237 and Ser160 residues were also maintained in both minima. However, it is important to note that the Asp209 residue suffers the most conformational changes and the Arg280 residue also showed a variation in its position due to the alteration of PET configuration to planar to L-shape. The π - π interaction between Trp185 and the ring of the first monomer was maintained in both minima (Figure S11B). Interestingly, the connecting β 1- β 2 loop (loop 3) variations were not observed for these minimum conformations.

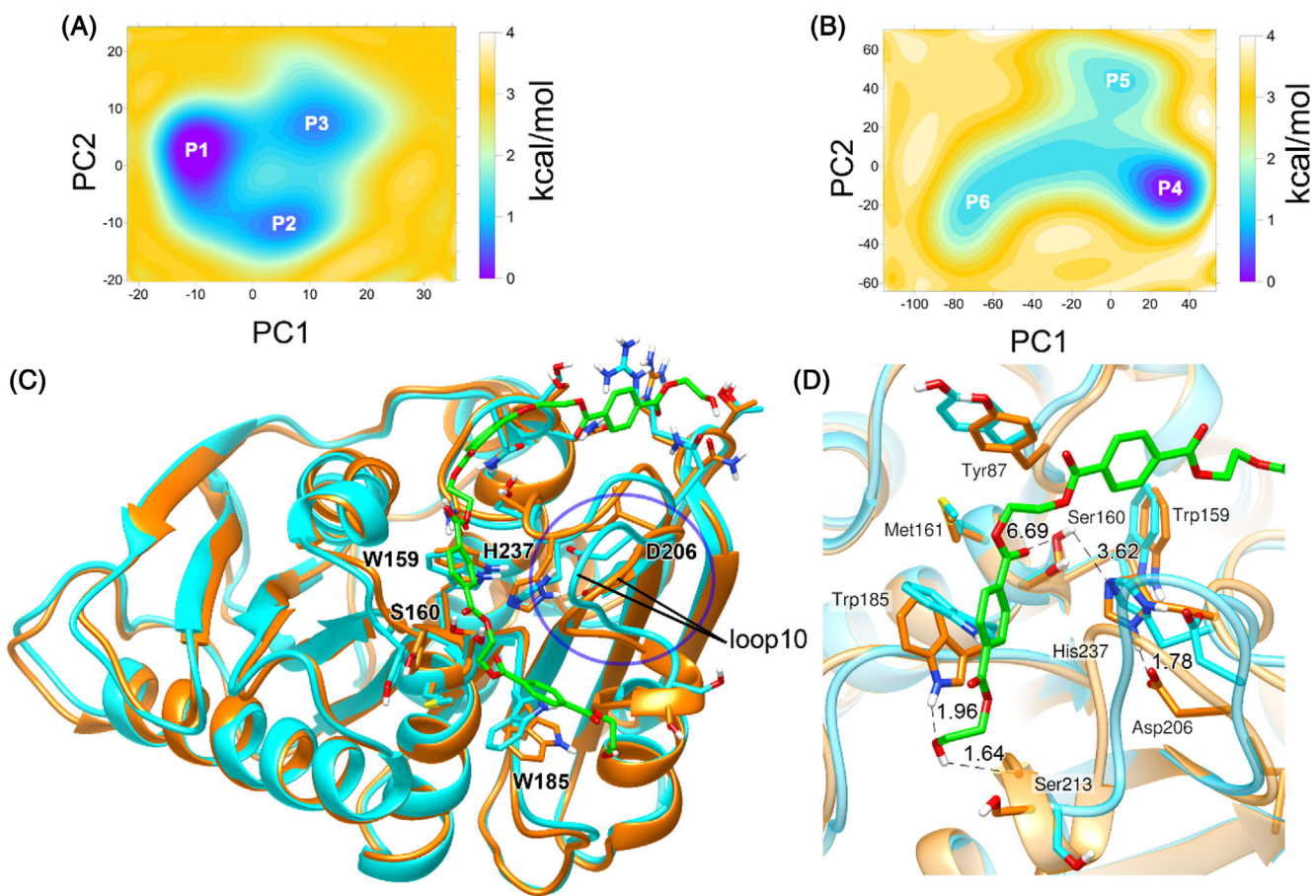


FIGURE 5 FEL analysis of different *IsPETase* states (P1 vs P4) in their native conformations. A, FEL of unbound state. B, FEL of the bound state. C, Structural comparison between the minimal structures of *IsPETase* in the unbound state (P1, blue) and the PETase in the bound state (P4, orange) complexed with PET (green). The blue circle indicates the main conformational change between the two *IsPETase* states. The $\beta_1\text{-}\beta_2$ connecting loop is represented by Loop10. D, Intermolecular interactions formed between the PET structure and the residues Trp159, Ser160, and His237 of the *IsPETase* binding site

4 | CONCLUSIONS

We have demonstrated a consistent model for simulating the *IsPETase* complexed with the PET, and its binding mode, which is in agreement with the currently available information in the literature. Our proposed model for PET binding mode can explain the conformational changes of protein structure and may be useful for the development of new biocatalysts, as well as for the elucidation of the catalytic mechanism of plastic recycling enzymes. The determination of the binding mode of PET into the active site of *IsPETase* is important for understanding the catalytic mechanism of this enzyme. Our results also revealed that the $\beta_1\text{-}\beta_2$ connecting loop is very flexible and may be targeted for mutagenesis to increase the *IsPETase* stability. Overall, the results provide useful benchmarks for further engineering of *IsPETase* structure aiming the recycling of plastic polymers using this biological system.

ACKNOWLEDGMENTS

Authors would like to thank the Laboratório Nacional de Computação Científica (LNCC) for providing access to the Santos Dumont

Supercomputer for scientific calculations, the Conselho Nacional de Desenvolvimento Científico e Tecnológico (CNPq, grant numbers: 402572/2018-1, 306014/2018-1, and 308254/2017-1), the Spanish Ministerio de Ciencia e Innovación (grant PGC2018-094852-B-C21), the Generalitat Valenciana (grant AICO/2019/195), and Universitat Jaume I (grant UJI-B2020-03) for financial support. K.S and A.M.S are also grateful for the scholarship from the Brazilian funding agency Coordenação de Aperfeiçoamento de Pessoal de Nível Superior (CAPES, grant number: 88882.466102/2019-01 and 88887.599350/2021-00, respectively).

CONFLICT OF INTEREST

The authors declare no conflict of interest regarding the publication of the manuscript. The funders had no role in the design of the study; in the collection, analyses, or interpretation of data; in the writing of the manuscript, or in the decision to publish the results.

AUTHOR CONTRIBUTION

Clauber Henrique Souza da Costa: Investigation. **Alberto M. dos Santos:** Investigation. **Cláudio Nahum Alves:** Data curation. **Sérgio Martí:**

Conceptualization, data curation, writing manuscript. **Vicent Moliner:** Conceptualization, data curation, writing manuscript. **Kauê Santana:** Conceptualization, data curation, writing manuscript. **Jerônimo Lameira:** Conceptualization, writing manuscript. All authors have read and agreed to the published version of the manuscript.

PEER REVIEW

The peer review history for this article is available at <https://publons.com/publon/10.1002/prot.26155>.

DATA AVAILABILITY STATEMENT

The data that support the findings of this study are available from the corresponding author upon reasonable request.

ORCID

Kauê Santana  <https://orcid.org/0000-0002-2735-8016>

Jerônimo Lameira  <https://orcid.org/0000-0001-7270-1517>

REFERENCES

1. Restrepo-Flórez JM, Bassi A, Thompson MR. Microbial degradation and deterioration of polyethylene - a review. *Int Biodeterior Biodegr.* 2014;88:83-90. <https://doi.org/10.1016/j.ibiod.2013.12.014>.
2. Brunner I, Fischer M, Rüthi J, Stierli B, Frey B. Ability of fungi isolated from plastic debris floating in the shoreline of a lake to degrade plastics. *PLoS One.* 2018;13:e0202047. <https://doi.org/10.1371/journal.pone.0202047>.
3. Jambeck JR, Geyer R, Wilcox C, et al. Plastic waste inputs from land into the ocean. *Science.* 2015;347:768-771. <https://doi.org/10.1126/science.1260352>.
4. Barnes DKA, Galgani F, Thompson RC, Barlaz M. Accumulation and fragmentation of plastic debris in global environments. *Philos Trans R Soc Lond B Biol Sci.* 2009;364:1985-1998. <https://doi.org/10.1098/rstb.2008.0205>.
5. Picó Y, Barceló D. Analysis and prevention of microplastics pollution in water: current perspectives and future directions. *ACS Omega.* 2019;4:6709-6719. <https://doi.org/10.1021/acsomega.9b00222>.
6. Yoshida S, Hiraga K, Takehana T, et al. A bacterium that degrades and assimilates poly(ethylene terephthalate). *Science.* 2016;351:1196-1199. <https://doi.org/10.1126/science.aad6359>.
7. Tournier V, Topham CM, Gilles A, et al. An engineered PET depolymerase to break down and recycle plastic bottles. *Nature.* 2020;580:216-219. <https://doi.org/10.1038/s41586-020-2149-4>.
8. Chen Z, Wang Y, Cheng Y, et al. Efficient biodegradation of highly crystallized polyethylene terephthalate through cell surface display of bacterial PETase. *Sci Total Environ.* 2020;709:136138. <https://doi.org/10.1016/j.scitotenv.2019.136138>.
9. Son HF, Cho IJ, Joo S, et al. Rational protein engineering of thermostable PETase from Ideonella sakaiensis for highly efficient PET degradation. *ACS Catal.* 2019;9:3519-3526. <https://doi.org/10.1021/acscatal.9b00568>.
10. Taniguchi I, Yoshida S, Hiraga K, Miyamoto K, Kimura Y, Oda K. Bio-degradation of PET: current status and application aspects. *ACS Catal.* 2019;9:4089-4105. <https://doi.org/10.1021/acscatal.8b05171>.
11. Tanasupawat S, Takehana T, Yoshida S, Hiraga K, Oda K. Ideonella sakaiensis sp. nov., isolated from a microbial consortium that degrades poly(ethylene terephthalate). *Int J Syst Evol Microbiol.* 2016; 66:2813-2818. <https://doi.org/10.1099/ijsem.0.001058>.
12. Palm GJ, Reisky L, Böttcher D, et al. Structure of the plastic-degrading Ideonella sakaiensis MHETase bound to a substrate. *Nat Commun.* 2019;10:1717. <https://doi.org/10.1038/s41467-019-09326-3>.
13. Joo S, Cho IJ, Seo H, et al. Structural insight into molecular mechanism of poly(ethylene terephthalate) degradation. *Nat Commun.* 2018; 9:382. <https://doi.org/10.1038/s41467-018-02881-1>.
14. Han X, Liu W, Huang JW, et al. Structural insight into catalytic mechanism of PET hydrolase. *Nat Commun.* 2017;8:2106. <https://doi.org/10.1038/s41467-017-02255-z>.
15. Fecker T, Galaz-Davison P, Engelberger F, et al. Active site flexibility as a Hallmark for efficient PET degradation by *I. sakaiensis* PETase. *Biophys J.* 2018;114:1302-1312. <https://doi.org/10.1016/j.bpj.2018.02.005>.
16. Dimarogona M, Nikolaivits E, Kanelli M, Christakopoulos P, Sandgren M, Topakas E. Structural and functional studies of a *Fusarium oxysporum* cutinase with polyethylene terephthalate modification potential. *Biochim Biophys Acta - Gen Sub.* 1850;2015: 2308-2317. <https://doi.org/10.1016/j.bbagen.2015.08.009>.
17. Müller RJ, Schrader H, Profe J, Dresler K, Deckwer WD. Enzymatic degradation of poly(ethylene terephthalate): rapid hydrolyse using a hydrolase from *T. fusca*. *Macromol Rapid Commun.* 2005;26:1400-1405. <https://doi.org/10.1002/marc.200500410>.
18. Nimchua T, Punnapayak H, Zimmermann W. Comparison of the hydrolysis of polyethylene terephthalate fibers by a hydrolase from *Fusarium oxysporum* LCH I and *Fusarium solani* f. sp. *pisi*. *Biotechnol J.* 2007;2:361-364. <https://doi.org/10.1002/biot.200600095>.
19. Liebminger S, Eberl A, Sousa F, et al. Hydrolysis of PET and bis(benzoyloxyethyl) terephthalate with a new polyesterase from *Penicillium citrinum*. *Biocatal Biotransf.* 2007;25:171-177. <https://doi.org/10.1080/10242420701379734>.
20. Ribitsch D, Acerro EH, Greimel K, et al. A new esterase from *Thermobifida halotolerans* hydrolyses polyethylene terephthalate (PET) and polylactic acid (PLA). *Polymers (Basel).* 2012;4:617-629. <https://doi.org/10.3390/polym4010617>.
21. Sulaiman S, Yamato S, Kanaya E, et al. Isolation of a novel cutinase homolog with polyethylene terephthalate-degrading activity from leaf-branch compost by using a metagenomic approach. *Appl Environ Microbiol.* 2012;78:1556-1562. <https://doi.org/10.1128/AEM.06725-11>.
22. Herrero Acerro E, Ribitsch D, Steinkellner G, et al. Enzymatic surface hydrolysis of PET: effect of structural diversity on kinetic properties of cutinases from *Thermobifida*. *Macromolecules.* 2011;44:4632-4640. <https://doi.org/10.1021/ma200949p>.
23. Kitadokoro K, Thumarat U, Nakamura R, et al. Crystal structure of cutinase Est119 from *Thermobifida alba* AHK119 that can degrade modified polyethylene terephthalate at 1.76 Å resolution. *Polym Degrad Stab.* 2012;97:771-775. <https://doi.org/10.1016/j.polymdegradstab.2012.02.003>.
24. Austin HP, Allen MD, Donohoe BS, et al. Characterization and engineering of a plastic-degrading aromatic polyesterase. *Proc Natl Acad Sci U S A.* 2018;115:E4350-E4357. <https://doi.org/10.1073/pnas.1718804115>.
25. Liu B, He L, Wang L, et al. Protein crystallography and site-direct mutagenesis analysis of the poly(ethylene terephthalate) hydrolase petase from *Ideonella sakaiensis*. *Chembiochem.* 2018;19:1471-1475. <https://doi.org/10.1002/cbic.201800097>.
26. Billig S, Oeser T, Birkemeyer C, Zimmermann W. Hydrolysis of cyclic poly(ethylene terephthalate) trimers by a carboxylesterase from *Thermobifida fusca* KW3. *Appl Microbiol Biotechnol.* 2010;87:1753-1764. <https://doi.org/10.1007/s00253-010-2635-y>.
27. Roth C, Wei R, Oeser T, et al. Structural and functional studies on a thermostable polyethylene terephthalate degrading hydrolase from *Thermobifida fusca*. *Appl Microbiol Biotechnol.* 2014;98:7815-7823. <https://doi.org/10.1007/s00253-014-5672-0>.
28. Chen CC, Han X, Ko TP, Liu W, Guo RT. Structural studies reveal the molecular mechanism of PETase. *FEBS J.* 2018;285:3717-3723. <https://doi.org/10.1111/febs.14612>.

29. Kawai F, Kawabata T, Oda M. Current knowledge on enzymatic PET degradation and its possible application to waste stream management and other fields. *Appl Microbiol Biotechnol.* 2019;103:4253-4268. <https://doi.org/10.1007/s00253-019-09717-y>.
30. Wei R, Zimmermann W. Biocatalysis as a green route for recycling the recalcitrant plastic polyethylene terephthalate. *J Microbial Biotechnol.* 2017;10:1302-1307. <https://doi.org/10.1111/jm.12714>.
31. Jones BJ, Lim HY, Huang J, Kazlauskas RJ. Comparison of five protein engineering strategies for stabilizing an α/β -hydrolase. *Biochemistry.* 2017;56:6521-6532. <https://doi.org/10.1021/acs.biochem.7b00571>.
32. Cui Y, Chen Y, Liu X, et al. Computational redesign of a PETase for plastic biodegradation under ambient condition by the GRAPE strategy. *ACS Catal.* 2021;11:1340-1350. <https://doi.org/10.1021/acscatal.0c05126>.
33. Trott O, Olson AJ. AutoDock Vina: improving the speed and accuracy of docking with a new scoring function, efficient optimization, and multithreading. *J Comput Chem.* 2009;31:455-461. <https://doi.org/10.1002/jcc.21334>.
34. De Azevedo WFJ. Mol dock applied to structure-based virtual screening. *Curr Drug Targets.* 2010;11:327-334. <https://doi.org/10.2174/138945010790711941>.
35. Cole JC, JWM N, Taylor R. Protein-ligand docking and virtual screening with GOLD. In: Alvarez J, Shoichet B, eds. *Virtual Screening in Drug Discovery.* Boca Raton, FL: Taylor & Francis CRC Press; 2005: 379-415.
36. Case DA, Cheatham TE, Darden T, et al. The Amber biomolecular simulation programs. *J Comput Chem.* 2005;26:1668-1688. <https://doi.org/10.1002/jcc.20290>.
37. Li Y, Abberton BC, Kröger M, Liu WK. Challenges in multiscale modeling of polymer dynamics. *Polymers.* 2013;5:751-832. <https://doi.org/10.3390/polym5020751>.
38. Amari T, Ozaki Y. Generalized two-dimensional attenuated total reflection/infrared and near-infrared correlation spectroscopy studies of real-time monitoring of the initial oligomerization of bis(hydroxyethyl terephthalate). *Macromolecules.* 2002;35:8020-8028. <https://doi.org/10.1021/ma020723y>.
39. Gartner TE, Jayaraman A. Modeling and simulations of polymers: a roadmap. *Macromolecules.* 2019;52:755-786. <https://doi.org/10.1021/acs.macromol.8b01836>.
40. David CC, Jacobs DJ. Principal component analysis: a method for determining the essential dynamics of proteins. *Methods Mol Biol.* 2014;1084:193-226. https://doi.org/10.1007/978-1-62703-658-0_11.
41. Hornak V, Abel R, Okur A, Strockbine B, Roitberg A, Simmerling C. Comparison of multiple Amber force fields and development of improved protein backbone parameters. *Proteins.* 2006;65:712-725. <https://doi.org/10.1002/prot.21123>.
42. Frisch MJ, Nathan AJ, Scobell A. *Gaussian 09.* Wallingford CT: Gaussian Inc; 2009:2-3.
43. Mark P, Nilsson L. Structure and dynamics of the TIP3P, SPC, and SPC/E water models at 298 K. *J Phys Chem A.* 2001;105:9954-9960. <https://doi.org/10.1021/jp003020w>.
44. Gilson MK, Given JA, Bush BL, McCammon JA. The statistical-thermodynamic basis for computation of binding affinities: a critical review. *Biophys J.* 1997;72:1047-1069. [https://doi.org/10.1016/S0006-3495\(97\)78756](https://doi.org/10.1016/S0006-3495(97)78756).
45. Roux B, Nina M, Pomès R, Smith JC. Thermodynamic stability of water molecules in the bacteriorhodopsin proton channel: a molecular dynamics free energy perturbation study. *Biophys J.* 1996;71:670-681. [https://doi.org/10.1016/S0006-3495\(96\)79267-6](https://doi.org/10.1016/S0006-3495(96)79267-6).
46. Boresch S, Tettinger F, Leitgeb M, Karplus M. Absolute binding free energies: a quantitative approach for their calculation. *J Phys Chem B.* 2003;107:9535-9551. <https://doi.org/10.1021/jp0217839>.
47. Mobley DL, Chodera JD, Dill KA. On the use of orientational restraints and symmetry corrections in alchemical free energy calculations. *J Chem Phys.* 2006;125:084902. <https://doi.org/10.1063/1.2221683>.
48. Palese LL. A random version of principal component analysis in data clustering. *Comput Biol Chem.* 2018;73:57-64. <https://doi.org/10.1016/j.compbiochem.2018.01.009>.
49. Costa CHS, Oliveira ARS, dos Santos AM, et al. Computational study of conformational changes in human 3-hydroxy-3-methylglutaryl coenzyme reductase induced by substrate binding. *J Biomol Struct Dyn.* 2019;37:4374-4383. <https://doi.org/10.1080/07391102.2018.1549508>.
50. da Costa CHS, Bichara TW, Gomes GC, et al. Unraveling the conformational dynamics of glycerol 3-phosphate dehydrogenase, a nicotinamide adenine dinucleotide-dependent enzyme of *Leishmania mexicana*. *J Biomol Struct Dyn.* 2020;39:1-12. <https://doi.org/10.1080/07391102.2020.1742206>.
51. Kumari P, Poddar R. A comparative multivariate analysis of nitrilase enzymes: an ensemble based computational approach. *Comput Biol Chem.* 2019;83:107095. <https://doi.org/10.1016/j.compbiochem.2019.107095>.
52. Neves Cruz J, da Costa KS, de Carvalho TAA, de Alencar NAN. Measuring the structural impact of mutations on cytochrome P450 21A2, the major steroid 21-hydroxylase related to congenital adrenal hyperplasia. *J Biomol Struct Dyn.* 2020;38:1425-1434. <https://doi.org/10.1080/07391102.2019.1607560>.
53. Li C, Chen S, Huang T, et al. Conformational changes of glutamine 5'-Phosphoribosylpyrophosphate Amidotransferase for two substrates analogue binding: insight from conventional molecular dynamics and accelerated molecular dynamics simulations. *Front Chem.* 2021;9:1-14. <https://doi.org/10.3389/fchem.2021.640994>.
54. Valente RP d P, Souza RC d, de Medeiros Muniz G, et al. Using accelerated molecular dynamics simulation to elucidate the effects of the T198F mutation on the molecular flexibility of the West Nile virus envelope protein. *Sci Rep.* 2020;10:9625. <https://doi.org/10.1038/s41598-020-66344-8>.
55. Fonseca ECM, da Costa KS, Lameira J, Alves CN, Lima AH. Investigation of the target-site resistance of EPSP synthase mutants P106T and T102I/P106S against glyphosate. *RSC Adv.* 2020;10:44352-44360. <https://doi.org/10.1039/DORA09061A>.
56. Grosso M, Kalstein A, Parisi G, Roitberg AE, Fernandez-Alberti S. On the analysis and comparison of conformer-specific essential dynamics upon ligand binding to a protein. *J Chem Phys.* 2015;142:245101. <https://doi.org/10.1063/1.4922925>.
57. Salmas RE, Yurtseven M, Durdag S. Investigation of inhibition mechanism of chemokine receptor CCR5 by micro-second molecular dynamics simulations. *Sci Rep.* 2015;5:13180. <https://doi.org/10.1038/srep13180>.
58. Liu Y, Chipot C, Shao X, Cai W. Edge effects control helical wrapping of carbon nanotubes by polysaccharides. *Nanoscale.* 2012;4:2584-2589. <https://doi.org/10.1039/c2nr11979j>.
59. Grant BJ, Rodrigues APCC, ElSawy KM, McCammon JA, Caves LSDD. Bio3d: an R package for the comparative analysis of protein structures. *Bioinformatics.* 2006;22:2695-2696. <https://doi.org/10.1093/bioinformatics/btl461>.
60. Karamzadeh R, Karimi-Jafari MH, Sharifi-Zarchi A, Chitsaz H, Salekdeh GH, Moosavi-Movahedi AA. Machine learning and network analysis of molecular dynamics trajectories reveal two chains of red-/ox-specific residue interactions in human protein disulfide Isomerase. *Sci Rep.* 2017;7:3666. <https://doi.org/10.1038/s41598-017-03966-5>.
61. Papaleo E, Mereghetti P, Fantucci P, Grandori R, De Gioia L. Free-energy landscape, principal component analysis, and structural clustering to identify representative conformations from molecular

- dynamics simulations: the myoglobin case. *J Mol Graph Model.* 2009; 27:889-899. <https://doi.org/10.1016/j.jmgm.2009.01.006>.
62. Wei R, Song C, Gräsing D, et al. Conformational fitting of a flexible oligomeric substrate does not explain the enzymatic PET degradation. *Nat Commun.* 2019;10:5581. <https://doi.org/10.1038/s41467-019-13492-9>.
63. Roe DR, Cheatham TE. PTRAJ and CPPTRAJ: software for processing and analysis of molecular dynamics trajectory data. *J Chem Theory Comput.* 2013;9:3084-3095. <https://doi.org/10.1021/ct400341p>.
64. Shao J, Tanner SW, Thompson N, Cheatham TE. Clustering molecular dynamics trajectories: 1. Characterizing the performance of different clustering algorithms. *J Chem Theory Comput.* 2007;3:2312-2334. <https://doi.org/10.1021/ct700119m>.
65. Calinski T, Harabasz J. Communications in statistics a dendrite method for cluster analysis. *Commun Stat.* 1974;3:1-27.
66. Davies DL, Bouldin DW. A cluster separation measure. *IEEE Trans Pattern Anal Mach Intell.* 1979;PAMI-1:224-227. <https://doi.org/10.1109/TPAMI.1979.4766909>.
67. Vesanto J, Alhoniemi E. Clustering of the self-organizing map. *IEEE Trans Neural Netw.* 2000;11:586-600. <https://doi.org/10.1109/72.846731>.
68. Speer N, Spiet C, Zell A. Biological cluster validity indices based on the gene ontology BT - advances in intelligent data analysis VI. In: Famili AF, Kok JN, Peña JM, Siebes A, Feedlers A, eds. Berlin, Heidelberg: Springer Berlin Heidelberg; 2005:429-439.
69. Ma Y, Yao M, Li B, et al. Enhanced poly(ethylene terephthalate) hydrolase activity by protein engineering. *Engineering.* 2018;4:888-893. <https://doi.org/10.1016/j.eng.2018.09.007>.
70. Knott BC, Erickson E, Allen MD, et al. Characterization and engineering of a two-enzyme system for plastics depolymerization. *Proc Natl Acad Sci.* 2020;117:25476-25485. <https://doi.org/10.1073/pnas.2006753117>.

SUPPORTING INFORMATION

Additional supporting information may be found online in the Supporting Information section at the end of this article.

How to cite this article: da Costa CHS, dos Santos AM, Alves CN, et al. Assessment of the PETase conformational changes induced by poly(ethylene terephthalate) binding. *Proteins.* 2021;89(10):1340-1352. <https://doi.org/10.1002/prot.26155>